Journal of Applied Physics

Effect of porosity and tortuosity of electrodes on carbon polymer soft actuators

Cite as: J. Appl. Phys. **123**, 014502 (2018); https://doi.org/10.1063/1.5007147
Submitted: 30 September 2017 . Accepted: 13 December 2017 . Published Online: 03 January 2018

Sunjai Nakshatharan S, Andres Punning, Urmas Johanson, and Alvo Aabloo

Effect of porosity and tortuosity of electrodes on carbon polymer soft actuators

Sunjai Nakshatharan S,[a] Andres Punning, Urmas Johanson, and Alvo Aabloo
Intelligent Materials and Systems Laboratory, University of Tartu, Institute of Technology, Tartu, Estonia

(Received 30 September 2017; accepted 13 December 2017; published online 3 January 2018)

This work presents an electro-mechanical model and simulation of ionic electroactive polymer soft actuators with a porous carbon electrode, polymer membrane, and ionic liquid electrolyte. An attempt is made to understand the effects of specific properties of the porous electrodes such as porosity and tortuosity on the charge dynamics and mechanical performance of the actuator. The model uses porous electrode theory to study the electrochemical response of the system. The mechanical response of the whole laminate is attributed to the evolution of local stresses caused by diffusion of ions (diffusion-induced stresses or chemical stresses). The model indicates that in actuators with porous electrode, the diffusion coefficient of ions, conductivity of the electrodes, and ionic conductivity in both electrodes and separator are altered significantly. In addition, the model leads to an obvious deduction that the ions that are highly active in terms of mobility will dominate the whole system in terms of resulting mechanical deformation direction and rate of deformation. Finally, to validate the model, simulations are conducted using the finite element method, and the outcomes are compared with the experimental data. Significant effort has been put forward to experimentally measure the key parameters essential for the validation of the model. The results show that the model developed is able to well predict the behavior of the actuator, providing a comprehensive understanding of charge dynamics in ionic polymer actuator with porous electrodes. *Published by AIP Publishing*. https://doi.org/10.1063/1.5007147

I. INTRODUCTION

Ionic electroactive polymer (IEAP) transducers are a type of electroactive polymer device belonging to the class of smart materials with applications focusing on soft actuators and sensors. The materials are well suited for microactuator applications due to their ability to generate a large strain of about 2% with a low voltage of 0.5–5 V.[1]

Among the IEAPs, the most known are the ionic polymer-metal composite (IPMC). It consists of a solvent-swollen ionomer film, which is plated on both sides with compliant electronically conductive electrodes.[2] The IPMC actuators are usually operated in water. Under applied electric field, the hydrated cations and water molecules pass through the nanochannels of ionomer and congregate on the surface of one electrode forming an electrical double layer. The imbalanced distribution of mass and charge leads to the deformation of the whole film.[3] With larger electrode surface area, the number of ions and water molecules near the electrodes is higher and hence leads to larger deformation. Even though this type of actuator is well studied, a wider deployment of these materials for applications is limited, mainly because of their complex manufacturing, limitation in obtaining large surface area, and unstable operation caused by evaporation and electrolysis of the solvent.[4] These disadvantages of the old type IPMC and the requirement of the large electrode surface area have led to the development of actuators with porous electrodes and nonvolatile electrolytes.

The most commonly used metals for the IPMC electrodes are gold or platinum, while the ionomer is Nafion or Flemion. The up-to-date materials of porous electrodes are mainly different allotropes of carbon: carbon nanotubes,[5,6] bucky carbon gels,[7] graphene,[8] carbon aerogel,[9] nanoporous carbon,[10] etc. Further, interesting hybrid materials based on 3D graphene-CNT-Ni[11] and sulfur and nitrogen Co-doped graphene electrode[12] are reported. The use of these active materials along with ionic liquid (IL) as the electrolyte has been studied extensively for actuator applications. The nonvolatile ionic liquids possess a large electrochemical window that allows the actuators to be operated at higher voltages in the open-air environment for a prolonged period of time.[13–15] In order to further prevent the leakage of electrolyte, there are attempts to develop laser-scribed reduced graphene oxide paper electrodes that greatly contribute to increasing the durability of the actuator for practical applications.[16]

A. Carbon polymer composite

In this work, we deal with the soft IEAP material with nanoporous carbon electrodes, polyvinylidene fluoride-*co*-hexafluoropropylene (PVdF-HFP) separator membrane and an ionic liquid as electrolyte. Nanoporous carbon which is derived from titanium carbide (CDC) possesses high surface area (1000–2000 m^2/g), controlled micropore volumes and pore size distributions, high electric double-layer capacitance (130 F/g and 90 F/cm^3 in nonaqueous solution), very good material stability, and chemical inertness.[17] The PVdF-HFP membrane has excellent thermal stability, high ionic conductance, chemical resistance, and mechanical property.[18]

[a]Author to whom correspondence should be addressed: sunjainakshatharan@gmail.com

Along with these superior properties of these materials, the fabrication process of this kind of actuator is also relatively simple, repeatable, scalable, and cost-effective.[19] Also this type of actuators can withstand more than ten thousand cycles without any delamination issues.[19] In terms of construction, this IEAP material is very similar to the double-layer capacitors and can be considered as a flexible supercapacitor.[10] Based on the construction, we denote this IEAP material as Carbon Polymer Composite (CPC).

This type of actuator differs from traditional IPMC mainly by the following two aspects:

1. The electrode is highly porous; hence, the ions do not just congregate near the electrode surface but rather intercalate into the electrode. Porosity and tortuosity effects play a significant role in the morphology of the electrodes and in the effective transport properties of the ions.
2. The polymer membrane is a non-ionomer. In IPMC, the anions are fixed to the backbone of the ionomer membrane; therefore, only the movement of mobile cations and water molecules causes the deformation. In CPC, both anions and cations are free to move. Here the deformation depends on the charge, mobility, size, diffusion coefficient, etc., of both types of ions.

The schematic representation of the CPC laminate and the Scanning Electron Microscope (SEM) picture of the same are shown in Figs. 1(a) and 1(b). The average size of the carbon particles used in the current work is about 10 μm. The electrolyte is ionic liquid (IL), particularly the 1-ethyl-3-methylimidazolium trifluoromethanesulfonate (EMIM-TfO), known as one of the most investigated ILs concerning air-operated IEAP actuators. The detailed description of the fabrication process of this IEAP material is given by Kaasik *et al.*[19]

B. Motivation

Considering the electromechanical modelling of the IEAP transducers, numerous models exist for the traditional IPMC actuators, which involve different approaches such as black box, grey box, and physics based models.[17] Considering only the physics based model, which is the topic of current interest, there exist models only for the aqueous IPMC actuators.[1–3,20–23] Here we bring a few examples: Nemat-Nasser and Li have proposed a model that describes electromechanical transduction within the polymer.[23] Stalbaum *et al.* developed a physics based model based on coupling Nernst Planck Poisson equation and linear elastic theory to predict the deformation of the IPMC.[21] Wallmersperger *et al.* and Zhu *et al.* also proposed a similar multiphysics model based on the NPN equation.[1,3,22] However, these models consider only charge dynamics within the actuator and do not pay attention to the physical and electrical properties of the electrodes. The electrodes are considered only as flat conductors to provide an electric field. However, Porfiri showed that the electrodes do significantly affect the charge dynamics and hence the actuation performance of the actuator.[24] Also, Wang pointed that structural idealization of considering electrode as planar may lead to problematic predictions.[25] A few papers have attempted to explore this problem; Akle investigated the effect of conductive electrode particles' dispersion into the membrane by conducting simulation enabling the design of electrodes with a complicated pattern.[26] Chang *et al.* studied the effects of surface roughening on the mass transport and mechanical properties of IPMC.[27] Palmre calculated the mass transportation of IPMC with the Koch fractal electrode.[28] Shen *et al.* included the variable surface resistance of the electrode and showed that the model was able to predict dynamic performance of the actuator.[29] Nevertheless, a standardized result on the influence of electrode morphology is not yet available.

While IPMC has been thoroughly investigated, for the porous electrode based actuators only a few equivalent circuit or grey box models and control oriented transfer function models have been reported earlier.[30–35] As pointed out hereinabove, the electrodes of CPC are highly porous in nature. The effect of the tortuosity and porosity on the physical and electrical properties of the electrode and separator has not been observed in the prospect of actuator applications. For that reason, the models of IPMC cannot be directly adapted to predict the performance of CPC.

In this work, we focus on developing a physics based model that includes porous electrode theory. The resulting finite element simulations help understanding influence of

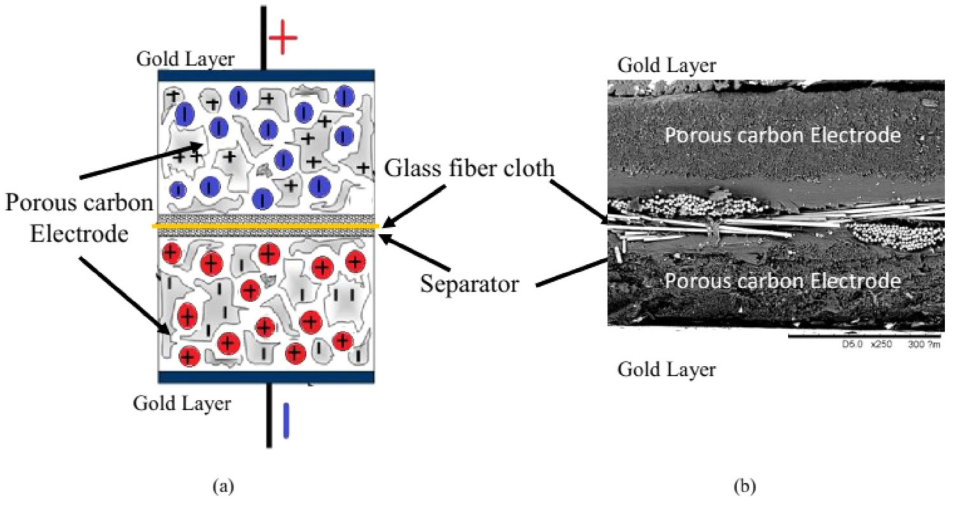

FIG. 1. (a) Graphical representation of the actuator. (b) Electron micrograph image.

the porous nature of the electrodes on the performance of the actuator. We start with describing the ion migration under electric field by combining the Nernst-Planck equation, Poisson's equation, and Navier-Stokes equation. The effective conductivity accounting the effect of porosity and tortuosity is involved using Bruggeman relation. Finally, applying the charge and mass balance conditions leads to the electromechanical response of a defined CPC sample. For experimental verification, many parameters used in the modelling are measured onsite, while only a few parameters are collected from datasheets and other literature.

C. General considerations of the physics based modelling of CPC

Physics based modelling of CPC can be divided into two distinct parts: (a) the electrochemical response, i.e., ion transport process on the application of electrical potential and (b) resultant mechanical deformation of the actuator. In this work, it is assumed that the mechanical deformation will take place purely due to the generation of intercalation stress or diffusion-induced stress.

In the previously published models of IPMC[1,21,29] coupling between the electrochemical processes and mechanical deformation is realized using an experimentally determined constant that relates the charge and force. In this work, the deformation is predicted through the intercalation stress caused by ion transportation and resulting volumetric swelling of the electrode. With this assumption, the strain is directly proportional to the resulting concentration gradient of the ions, while the constant of proportionality is the coefficient of swelling. This assumption (a) attributes a direct physical meaning to the coupling coefficient and (b) couples directly the electrochemical response and mechanical response for the multiphysics simulation.

Concerning the electrochemical response, the diffusion, convection, and migration of charged particles are commonly described with the NPN equation. The transport processes depend mainly on the properties of the ions, such as mobility, diffusion coefficient, and conductivity of ions and active carbon particles. The ionic conductivity and mobility are directly related to the diffusion coefficient of ions although the relationship between the physical properties of the electrode and separator and their relationship to the diffusion of ions have not been discussed in the former actuator applications.

Transfer of ions through the porous electrodes and membrane is the key factor in the design of actuators to achieve the optimum performance in terms of force and displacement. A number of spatial parameters of the porous media influence the diffusion coefficient and ionic conductivity; the most important of which are size and shape of particles, size and shape of pores, porosity, and tortuosity. For a specific CDC, the size and shape of particles are predetermined; hence, the porosity of the electrodes is a key design parameter. The term porosity is defined as the ratio of the volume of empty space to that of the total volume of the electrode. Electrolyte, binders, and other solvents usually occupy this empty space. The resultant structure of the electrode is a matrix of active carbon particles and electrolyte mixture. The term tortuosity is the arc-chord ratio of the diffusion length of ions L' to the displacement L. In other words, it can be considered as equivalent to resistance to the flow of ions through the electrode.

With a highly porous electrode, it is possible to obtain very low tortuosity, but the actuation performance will be low. Since the actuation is proportional to available active surface area, with the highly porous electrode, there is limited electrode material within the same volume as shown in Fig. 2(a). On the other hand, low porosity corresponds to high tortuosity, resulting in non-utilization of the available surface area efficiently; ions will not be able to access all the available electrode material through the limited pores as shown in Fig. 2(b).

Finding the optimal combination of porosity and tortuosity is a key criterion in gaining the maximum performance of the CPC actuator. Also, the thickness of the electrode has a direct relation to tortuosity which in turn depends on porosity. Generally, an actuator with thicker electrodes generates higher stress but responds slower due to increased tortuosity. Again, the situation can be considered as a design challenge to obtain optimum thickness with reduced tortuosity by designing 3-D architectured electrode with defined porosity.[36] The relation between the thickness of electrode, porosity, tortuosity, and performance of an actuator is beyond the scope of the current paper. The model given in this work provides the fundamental relationship with porosity and transport properties of the ions.

The model is rather complicated and involves many parameters (see Nomenclature).

II. ELECTROCHEMICAL RESPONSE

The underlying phenomenon of the actuator behavior is based on ion migration. Under electric field, this transport process is described using the Nernst-Planck equation[2]

$$\vec{J}_i = -D_i\vec{\nabla}c_i - \frac{z_iF}{RT}D_ic_i\vec{\nabla}\Phi_2 + c_i\vec{u},\ (i = +, -). \quad (1)$$

The equation relates ion molar flux for ionic species i to its concentration, electric potential, and the fluid velocity at any

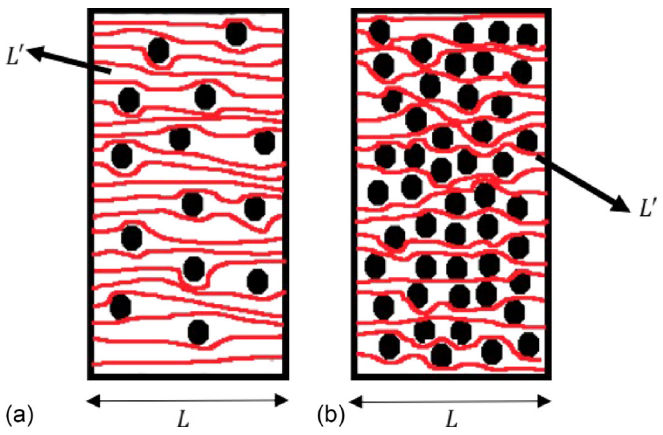

FIG. 2. Porosity-tortuosity models. (a) High porosity, low tortuosity and (b) low porosity, high tortuosity.

point within the domain. In applying the Nernst-Planck equation to ionic solution or liquid, the electric potential Φ_2 will be determined by the charge density within the domain. Mathematically, this can be expressed using the Poisson's equation

$$\nabla^2\Phi_2 = -\frac{\eta_e}{\varepsilon\varepsilon_o}, \tag{2}$$

where the charge density is given by

$$\eta_e = e(c_+ - c_-). \tag{3}$$

In order to evaluate the fluid velocity component u, the Navier-Stokes equation with the assumption that flux flow is laminar is used. The velocity of the flux is given by

$$\rho_p \frac{\partial u}{\partial t} + \rho_p\, u.\nabla u = -\nabla p + \nabla.\left(\mu\left(\nabla u + (\nabla u)^T\right) + F_l. \tag{4}$$

A portion of the fluid is pulled along as the ions within that portion are subject to the electric forces. The force acting upon the fluid is given by

$$F_l = (c_+ - c_-)F(\nabla\Phi_2). \tag{5}$$

A. Application of porous electrode theory

The two main factors that determine the effective ion transport through the porous electrode are the tortuosity and porosity.[37] Mathematically, tortuosity is given by

$$\tau = \frac{L'}{L}. \tag{6}$$

The tortuosity effects are not only limited to the electrode but it also has its influence on the separator or PVdF-HFP membrane.[38] The factors determining tortuosity are carbon particle size, ions size, membrane porous size, dispersity of particles, shape anisotropy, thickness of the electrode, etc.

Porosity is given by

$$\in = \frac{V_{empty}}{V_T}. \tag{7}$$

Bruggeman relation[37] gives the relationship between porosity and tortuosity as

$$\tau = \in^{-\beta}. \tag{8}$$

Ideally, the Bruggeman exponent β is equal to 1/2. In this work, we use an experimental image-based technique to measure the exact values of tortuosity directly; therefore, the β deviates from that value.

The effective conductivity of the porous electrode includes both conductivity of active particles and the spaces occupied by ionic liquid resulting in forming a matrix of active material and electrolyte.[39,40] The effective conductivity accounting for the effect of porosity and tortuosity can be approximated as

$$\rho_e = \frac{(1-\in)\rho}{\tau}. \tag{9}$$

The current conduction in the solid electrode phase by using Ohm's law is

$$i_1 = -\rho_e\nabla\Phi_1. \tag{10}$$

The ionic current due to the charge carried by ionic species is obtained by summing the currents of both ionic species

$$i_2 = F\sum_i z_i J_i. \tag{11}$$

Substituting ion flux of each species, Eq. (1) in Eq. (11) and considering the effect of tortuosity and porosity yields that the ionic current is

$$i_2 = -\rho_b\nabla\Phi_2 - z_iF(D_{eff+} - D_{eff-}) \in \nabla c_i + \left(\sum_i c_iF\vec{u}\right). \tag{12}$$

Here, D_{eff+}, D_{eff-} are the new effective diffusivities of cations and anions due to the porosity effect in the porous medium and are given by

$$D_{eff\,i} = D_i\frac{\in}{\tau}. \tag{13}$$

The new effective conductivity of the electrolyte in the bulk medium is given by

$$\rho_b = F^2\sum_i \frac{z_i^2 D_{effi}c_i}{RT}. \tag{14}$$

B. Charge and material balance conditions

The overall charge balance[41] is given by

$$\nabla\cdot i_1 + \nabla\cdot i_2 = 0. \tag{15}$$

At the interface between the matrix and the solution, the rate of change of the double layer charge[42] is given by the phenomenological relation

$$\nabla\cdot i_1 = -\nabla\cdot i_2 = -aC\frac{\partial(\Phi_1 - \Phi_2)}{\partial t}. \tag{16}$$

For various pore geometries, the specific surface area is given by

$$a = \frac{(1+\delta)\in}{r}. \tag{17}$$

Here,

$\delta = 2$ spheres,
$\delta = 1$ cylinders,
$\delta = 0$ slabs.

$\nabla\cdot i$ is the divergence of the current density in the matrix and represents the flow of current from the solution to the matrix phase.[43] This equation represents that ionic adsorption is approximated as a capacitive process. Finally, the material balance for the electrolyte[42] gives rise to the conservation equation

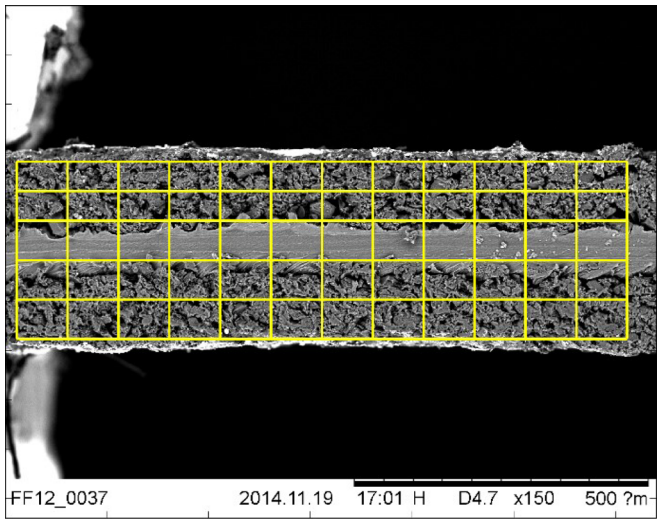

(a)

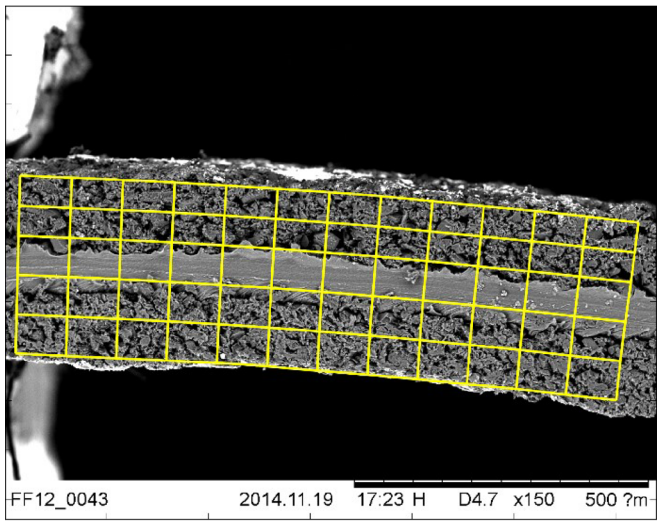

(b)

FIG. 3. Actuator SEM images. (a) Disengaged state. (b) Bending under voltage.

$$\in \frac{\partial c_i}{\partial t} = -\nabla j_i + R_i, \tag{18}$$

where R_i is the source term that represents the electrochemical reaction kinetics. For faradic processes usually Butler-Volmer and Tafel expressions are used to represent electrochemical reactions. But the CPC actuator operation is assumed purely to be non-faradic and capacitive. Thus, through the phenomenological relation, the double layer contribution and thereby the very high charge transfer are accounted. It is expressed as

$$R_i = -\frac{aC}{z_i F}\frac{\partial(\Phi_1 - \Phi_2)}{\partial t}. \tag{19}$$

C. Mechanical response

Generated stress and the resulting strain in the electrode is one of the highly studied areas in many fields including lithium-ion batteries and supercapacitors. Generally, stress generated in the electrode is a factor of performance degradation in batteries. However, in the case of flexible actuators, obtaining large strain and stress is a desired factor. Recently Gawith *et al.* studied electrochemical stiffness in lithium-ion batteries and concluded stress scales with lithiation/de-lithiation rate and strain scales with capacity.[44] Previously we have studied bending strain by *in situ* comparisons of scanning electron microscope micrographs for the bending actuator using a digital image correlation methodology.[45] In the work, we developed a technique for determining the factual deformations of the IEAP actuators under SEM. The actuators are spatially marked with factual regions. When actuated, the bending causes change in the volume of the regions. By comparing the volume change in each factual region, the change in volume of the actuator in each region can be visualized. The results depict expansion and shrinkage in volume of the electrode as the ions intercalate and result in subsequent bending. Figure 3 depicts the SEM images of the actuator under normal and actuated state, and Fig. 4 depicts the measured volumetric strain of the actuator along the thickness for a single square pulse.

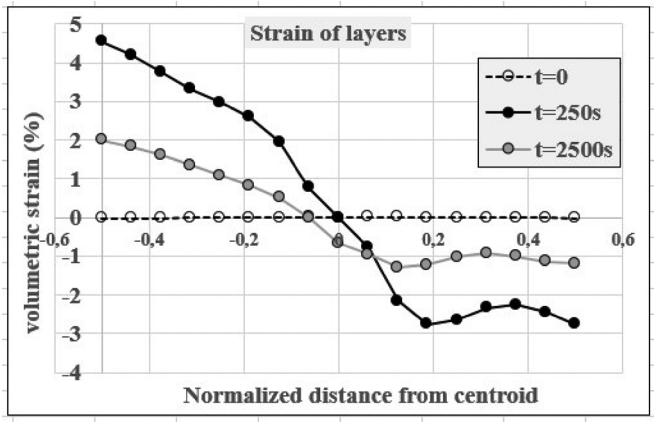

FIG. 4. The volumetric strain of CPC actuator driven with 2.8 V in vacuum.

From this understanding, in this work the mechanical model thereby the bending strain is accounted due to volumetric swelling of the electrodes. The theoretical assumption of stress generation in the mechanical model is accounted due to stress generation as a result of intercalation of ions. As discussed before, similar models of IPMC introduce a coupling constant between the electrochemical processes and mechanical deformation. The mechanical model introduced here relates directly to the concentration gradient and swelling of electrodes.

The constitutive relation, Hooke's law, was used to relate stress and strain in the actuator

$$\sigma = E\varepsilon. \tag{20}$$

The overall total stress generated in the material is given by

$$\sigma_T = \sigma_M - \sigma_{in}. \tag{21}$$

This relation indicates that the mechanical stress acts in the direction opposite to that of intercalation stress.

The intercalation stress is directly related to strain caused by swelling of the electrode

$$\sigma_{In} \propto \varepsilon_{in}. \tag{22}$$

The ε_{in} is the strain generation caused due to ion intercalation and resulting mass imbalance as given in Eq. (23). Mass imbalance is caused due to concentration difference of total migrating cations and anions

$$\varepsilon_{in} \propto (C_+ - C_-), \tag{23}$$

$$\varepsilon_{in} = \beta_{ss} M_s (C_+ - C_-), \tag{24}$$

or

$$\varepsilon_{in} = \beta_{ss} M_s \Delta C_{diff}, \tag{25}$$

where β_{ss} is swelling coefficient relating strain and ion concentration. This model can be used to predict the deformation direction based on the properties of cations and anions. The relation (24) or (25) is capable to predict such a deformation since it relates the concentration of ions, which in turn depends on the properties of ions.

The actuator can be either cation or anion driven. The diffusion coefficient, size of ions, and pore channels decide the respective movement of ions and thereby deformation direction. One more argument can be assumed here, which is that the ions that diffuse faster will dominate the whole system, since the ions that move first cause expansion of one electrode by occupying the pore channels. This expansion of one electrode due to intercalation makes the other electrode to shrink. The shrinking of electrode causes the subsequent closing of the pore channels for the counter ions. The narrow pore channels block the other ions to intercalate further into the electrode and stop the transport process. A very slow back relaxation process (bending in opposite direction after initial bending) that is typical in this kind of materials can be related to these counter ions that diffuse later and slowly.

The stress-strain relation for the material is given as

$$\begin{bmatrix} \sigma_{xx} \\ \sigma_{yy} \\ \sigma_{xy} \end{bmatrix} = \frac{E}{(1+\upsilon)(1-2\upsilon)} \begin{bmatrix} (1-\upsilon) & \upsilon & 0 \\ \upsilon & (1-\upsilon) & 0 \\ 0 & 0 & (1-2\upsilon) \end{bmatrix} \begin{bmatrix} \frac{\partial u}{\partial x} \\ \frac{\partial v}{\partial y} \\ \frac{1}{2}\left(\frac{\partial u}{\partial y} + \frac{\partial v}{\partial x}\right) \end{bmatrix} - \frac{E\beta\Delta C_{diff}}{1-2\upsilon} \begin{bmatrix} 1 \\ 1 \\ 0 \end{bmatrix}. \tag{26}$$

Similar to assumption adapted for traditional IPMC material,[21,29] CPC is also assumed to be isotropic. Since the actuation is due to ions movement only in transverse direction, the loading is always in one direction (bending direction). Hence, the change in property along a different direction is neglected for simplification. Further, during parameter measurement, Young's modulus is experimentally determined only in the transverse direction by a three-point bending method rather than along the axial direction. Also, this assumption helps in excluding the demanding computation task.

The time-dependent deformation is given by the PDE

$$\rho_p \frac{\partial^2 u}{\partial t^2} - \nabla.\sigma = F. \tag{27}$$

It is beneficial to note that this mechanoelectrical modelling framework presented herein can be applied to different ionic actuators with the porous electrode and can be related to stress generation in energy storage in supercapacitors.

III. EXPERIMENTAL COMPARISON

The main parameters used in the modelling of the actuator are measured from each layer of the fabricated material. Other parameters, which are specified in Table I, are collected from datasheets and other literature.

A. Measurement of parameters

The porosity of the electrode is an important parameter considered in this model. It contributes to the difference between the traditional model of IPMC and the actuator made of the porous electrode. The porosity of the electrode, as well as the separator, is calculated by measuring bulk density, mass, and volume of each layer and by calculating the ratio of void volume divided by nominal volume in each layer.[38] The tortuosity of the electrode and the separator is measured by using the image-based technique using the differential effective medium refraction method. Scanning Electron Microscope (SEM) images as shown in Fig. 5 are used to measure the parameter.[37] Ionic conductivity is defined as a function of the concentration of ions.[41] The mechanical parameter Young's modulus is measured using the three-point bending method.[46] Initial concentration was calculated from determining the ionic liquid mass ratio in each layer of the composite through which number of moles in each layer is determined (number of moles = mass of ionic liquid/molar mass). With the number of moles known, dividing it by the volume calculated by measuring the dimensions of the actuator under test gives the concentration of the ions in the composite.

The coefficient of swelling is the parameter that relates the concentration of ions and bending strain of the actuator. This value is used as a fitting parameter and is optimized to fit the experimental and simulation output. The value that

TABLE I. Parameters used in the simulation.

Symbol	Quantity	Value	Units	Reference
Le	Carbon electrode thickness	118	μm	Measured
Ls	Separator thickness	42	μm	Measured
aC	Specific capacitance	26	F/cm^3	Ref. 14.
C_{ini}	Initial concentration	1100	mol/m^3	Calculated
D_i	Diffusion coefficient of cation	1.324×10^{-9}	m^2/s	Ref. 47.
D_i	Diffusion coefficient of anion	0.994×10^{-9}	m^2/s	Ref. 47.
$\in_e$	Porosity of electrodes	0.60	…	Measured
$\in_s$	Porosity of separator	0.55	…	Measured
ρ_e	Solid phase conductivity	50	mS/cm	Ref. 17.
τ_e	Tortuosity of electrode	1.79	…	Measured
τ_s	Tortuosity of separator	1.34	…	Measured
ρ_p	Density of ionic liquid	1385.9	kg/m^3	Ref. 48.
μ	Dynamic viscosity of ionic liquid	42.936	mPa·s	Ref. 49.
E	Young's modulus of CPC	371	MPa	Measured
M_s	Molar mass of ionic liquid	0.260	Kg/mol	Ref. 48.
β_{ss}	Coefficient of swelling	9.5×10^{-5}	m^3/kg	Fitting parameter

found to make the best match is $9.5 \times 10^{-5} \frac{\text{m}^3}{\text{kg}}$. Under this constant, simulation is performed at different voltages and the results are compared with experimental results. Substituting the measured porosity and tortuosity values into Eq. (13) reveals that the effective diffusion coefficient in the electrode $D_{eff\,i}$ reduces to about 33.5% to that of diffusion coefficient in bulk D_i and to about 41% in the separator. Ionic conductivity relates directly to the diffusion coefficient and will also reduce to 33.5% and 41%, respectively. The electronic conductivity in porous electrode ρ_e is reduced to 23% of the conductivity of solid carbon electrode ρ. These results show that the porosity of electrodes plays a very significant role in reducing ionic conductivity, electrode conductivity, and diffusion coefficient. All three parameters alter the charge dynamics which results in affecting the performance of the actuator. It is self-evident that the porosity of the electrodes needs to be considered as one of the design parameters to obtain the optimum performance of the actuator.

IV. DISCUSSION

The finite element simulations with COMSOL Multiphysics were carried out for an actuator with the following dimensions: length 4 cm, width 1 cm, and thickness 0.0278 cm. Both electrodes are 0.0118 cm thick and the thickness of the separator is 0.0042 cm. The results were verified through experimental measurements using a sample with identical dimensions. A National Instruments DAQ device interfaced with PC running MATLAB is used to collect the measurement results. The experiment is conducted at four different step voltages: 0.5 V, 1 V, 1.5 V, and 2 V. The measured parameters were the consumed current and mechanical displacement while strain is calculated from displacement.[45]

The applied input signal of 1 V is shown in Fig. 6(a) and the resulting current both from experimental and simulation is shown in Fig. 6(b). Under applied potential, ion transport causes the spatiotemporal distribution of charge density, and this distribution of charge density within the material gives

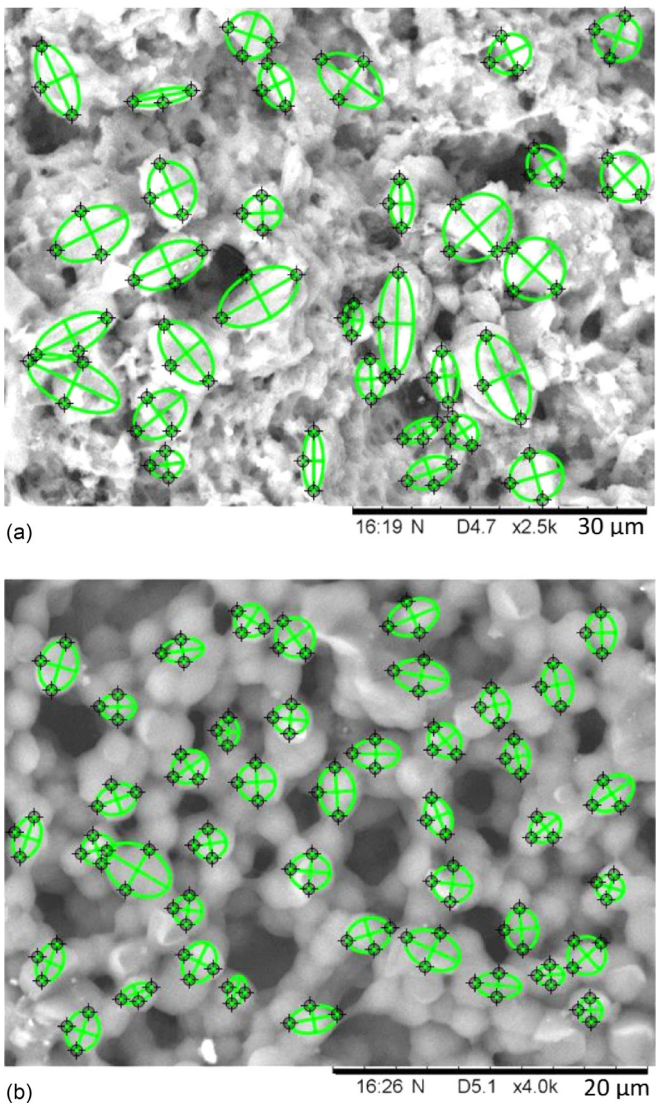

FIG. 5. Tortuosity measurement from SEM image. (a) Electrode and (b) separator.

rise to charges that collect at the faces of the electrodes. The charges that accumulate at the surface induce an electric current that can be measured across the thickness of the material and is denoted as isothermal transient ionic current.[1] Through simulation, this current response is simulated based on the time derivative of induced charge density and is presented and compared with experimentally measured current as shown in Fig. 6(b). The magnitude, charging, and discharging rate of output current from the simulation predicts the same behavior of experimentally measured current representing high fidelity of the presented electro-chemical model.

On application of the potential, the respective ions migrate towards the corresponding electrodes, i.e., cations move towards cathode and anions move towards the anode. Nevertheless, it does not make sense to expect that all ions will reach the electrodes; only a small fraction of ions takes part in the material transport. The result of this process is a concentration gradient of ions across the material. The resulting concentration gradient of ions can be plotted through simulation. The calculated ratio of cations and anions is plotted across the thickness of the actuator and is termed as normalized ion concentration. This parameter gives an overall understanding of the transport process in terms of actuation. The normalized ion concentration for applied 1 V is shown in Fig. 7. Under normal state, or with 0 V applied, the ratio is one, indicating a uniform concentration of ions across the material. On application of the potential, the transport process begins. The simulations reveal that the concentration ratio of migrating ions reaches a maximum of 1.4 in the cathode, which is nearly double that of in the anode, which is 0.78. The uneven concentration signifies that

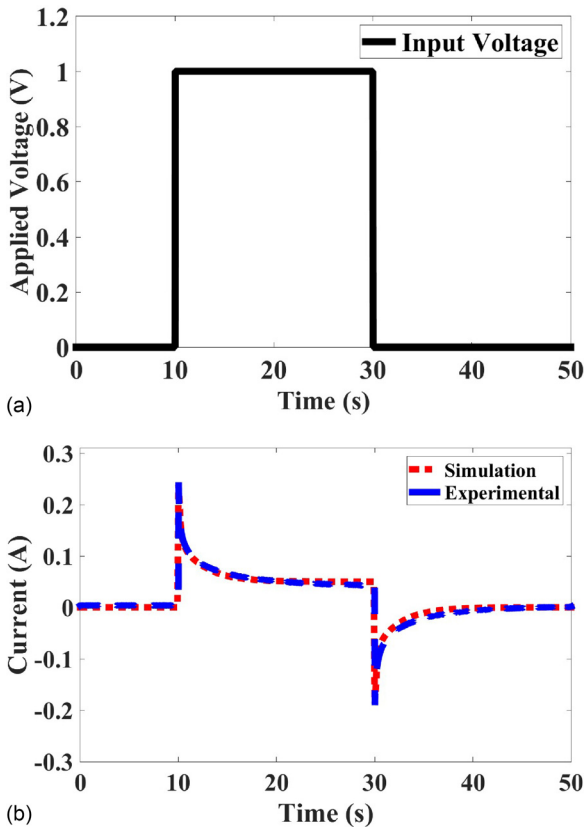

FIG. 6. (a) Applied potential and (b) current.

importance of cations in the transport process is much higher than the share of anions. The higher activity of one type of ions may be a result of the higher diffusion coefficient of cations, size of ions, etc., compared to that of anions. The material imbalance in the system results in expansion of cathode that reciprocates the shrinkage of the anode. Further, the shrinking anode causes the subsequent closing of pore channels. As the pore channels get narrower, porosity decreases and tortuosity increases, retarding the process of intercalation. As discussed above, the diffusion coefficient, size of ions, and pore channels

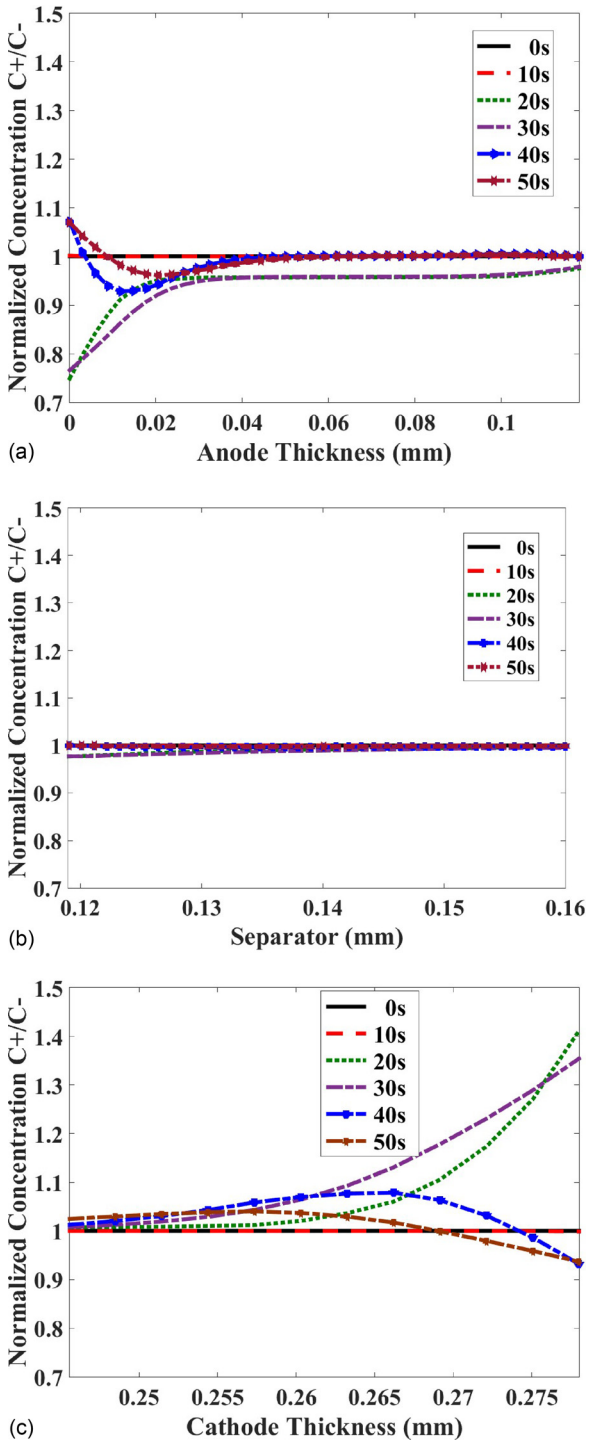

FIG. 7. Normalized ion concentration. (a) Anode, (b) separator, and (c) cathode.

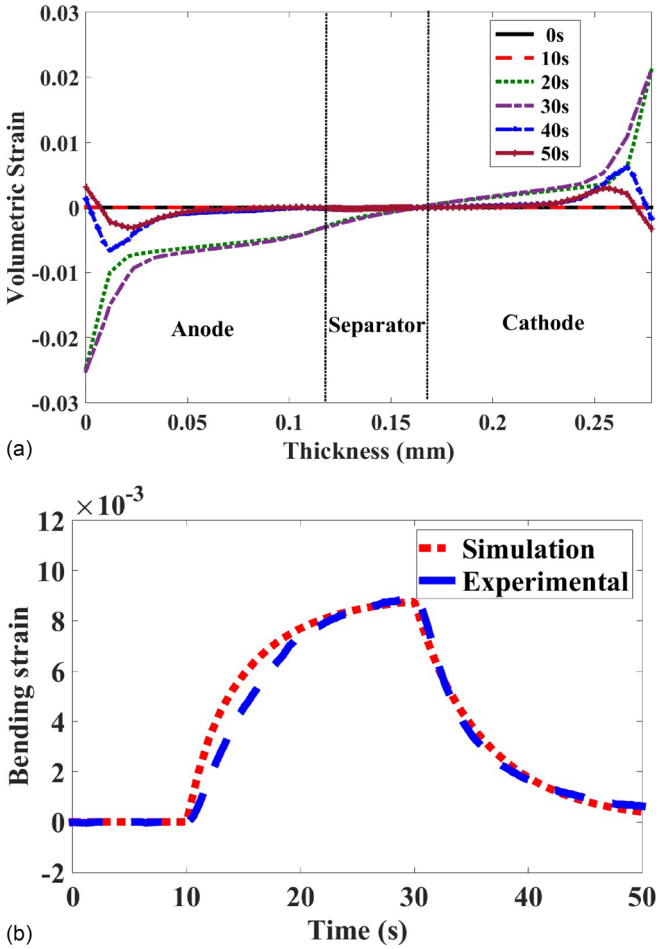

FIG. 8. (a) Volumetric strain and (b) bending strain.

determine the respective movement of ions and thereby the deformation direction. In the present scenario, the cations dominate the system and get accumulated at a higher rate than the anions. The strain generated in the mechanical model is attributed to the stress generated by effective ion intercalation. The correspondent volumetric swelling is described in Eq. (24).

The volumetric strain is a function of the resulting concentration gradient. The pattern of volumetric swelling follows a similar pattern to that of the concentration gradient

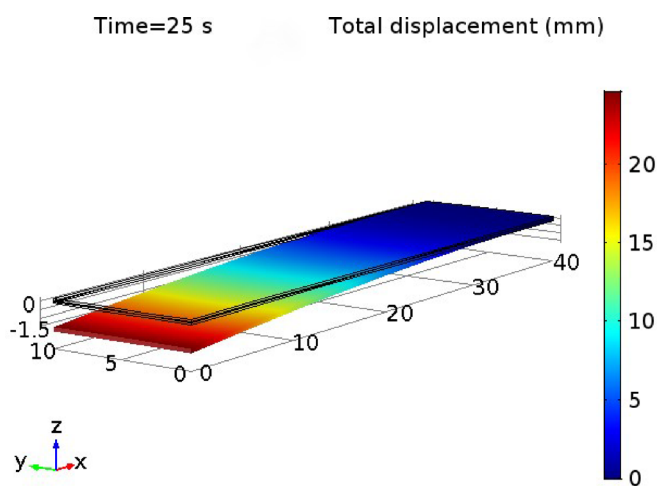

FIG. 9. Deformation of the actuator.

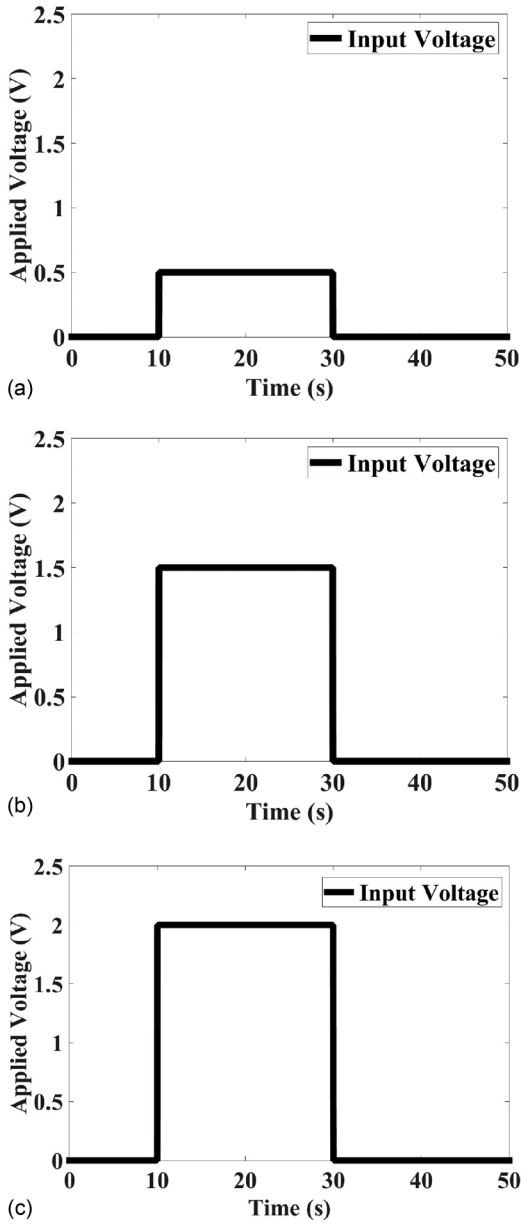

FIG. 10. Applied potential (a) 0.5 V, (b) 1.5 V, and (c) 2 V.

and is shown in Fig. 8(a). The simulation of the strain pattern across the actuator matches closely with the experimentally measured strain through the comparisons of scanning electron microscope micrographs experiment with the digital image correlation methodology.[45]

Comparison of simulated and experimental bending strain with respect to time is shown in Fig. 8(b). The simulation results show the good prediction of deformation matching with the experimental data. The slight mismatch can be accounted for different reasons such as hysteresis in the material, changes in porosity during deformation, non-linearity of the material, etc. A three-dimensional view of simulation of deformation of the actuator is shown in Fig. 9. With this model, the actuator can be coupled with other simulations employing the development of the actuator applications.

At other voltages, the simulation and experimental results are shown in Figs. 10–14. A good match is obtained between

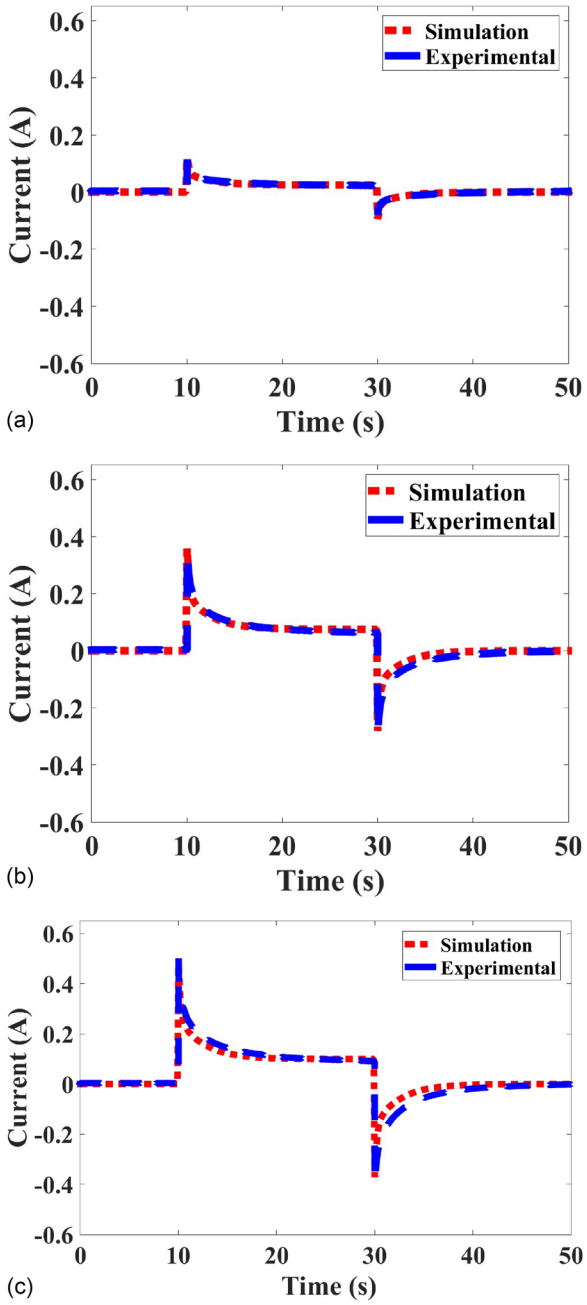

FIG. 11. Current profile (a) at 0.5 V, (b) at 1.5 V, and (c) at 2 V.

the predicted and experimental result at voltages of up to 1.5 V. At 2 V, Fig. 14(c) shows a considerable deviation between the simulation and experimental results. The mismatch of the model can be attributed to the onset of faradic reactions caused by electrolysis of water, which is not considered in the model. We have shown previously that ionic liquid in the actuator is hydrophilic in nature, and hence the actuator is highly influenced by surrounding humidity.[12] The electrolysis of water molecules that binds to the ionic liquids causes faradic reactions. Hence, this model can be applied to predict deformation with only non-faradic processes present.

V. CONCLUSION

In this work, electro-mechanical model and simulation of a soft actuator made of carbon polymer composite with porous carbon electrode are presented. The model comprises of two distinct parts, namely, electrochemical response and mechanical response. In the electrochemical response part, an attempt is made to understand the effects of porous electrode properties such as porosity and tortuosity on charge dynamics and in turn the performance of the actuator. It is calculated that in the porous electrode and separator the diffusion coefficient of ions reduces to 33.5% and 41%, respectively, compared to that of in bulk ionic liquid solution. The conductivity of the electrode decreases by a factor of 0.77 times to that of bulk conductivity. The ionic conductivity

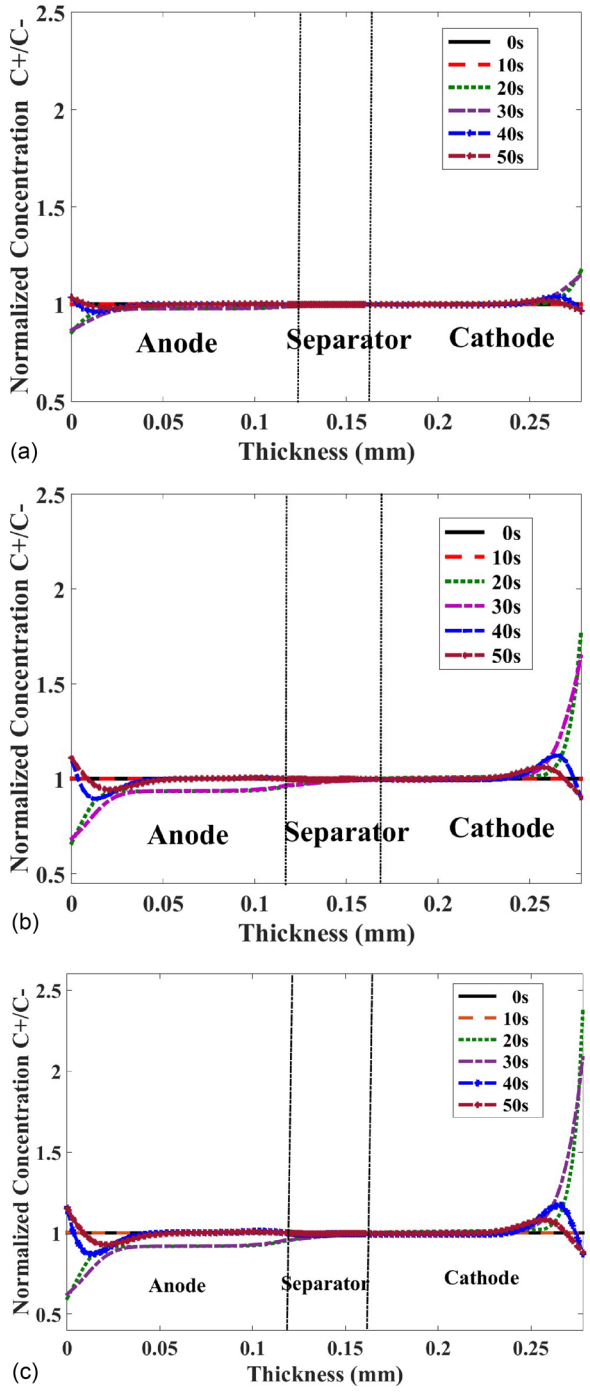

FIG. 12. Normalized ion concentration (a) at 0.5 V, (b) at 1.5 V, and (c) at 2 V.

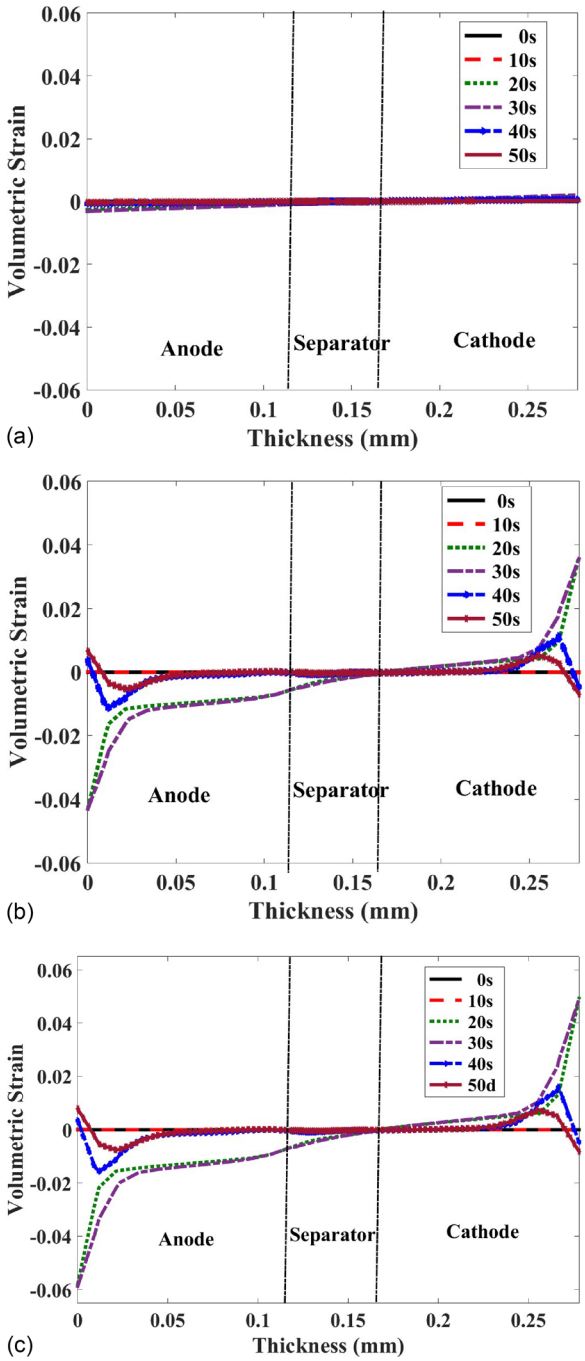

FIG. 13. Volumetric strain (a) at 0.5 V, (b) at 1.5 V, and (c) at 2 V.

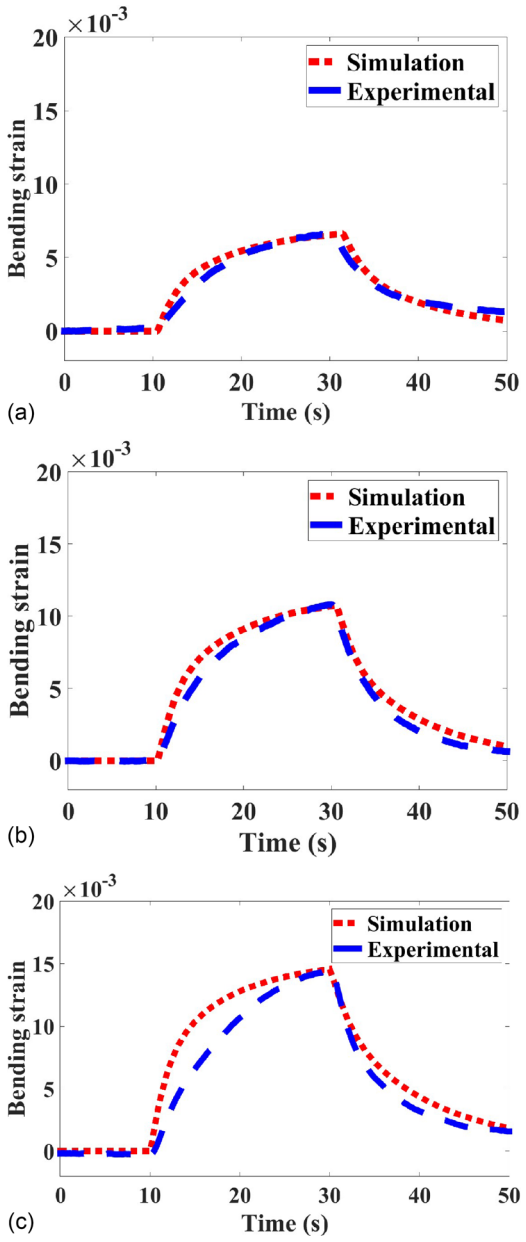

FIG. 14. Bending strain (a) at 0.5 V, (b) at 1.5 V, and (c) at 2 V.

drops by the same value as that of diffusion coefficient in both separator and electrode, respectively. In the mechanical response part, the deformation is attributed to volumetric swelling caused by the concentration gradient of ions as a result of intercalation process. It is found that for fixed pore channels and electrode porosity, the ions which are highly active in terms of mobility dominate the system and the resulting deformation direction and rate of deformation directly depends on these dominating ions. With this predicted model, simulation and experiments are conducted and the results are compared. The measured electric current and deformation of the actuator matches closely with the simulation results representing the high fidelity of the model. The model was successfully able to predict the behavior of the actuator till the onset of faradic reactions caused by electrolysis of water. The arguments in this paper can also be applied to other class of soft actuation devices such as ionic bucky gel actuators, carbon nanotube actuators, and ionic paper-based actuator. Overall, this study provides a comprehensive understanding of the behavior of ion driven deformation in soft actuators made of ionic polymer composites with the porous electrode.

ACKNOWLEDGMENTS

This work was funded by the H2020-MSCA-ITN grant of Marie-Sklodowska-Curie Innovative Training Network "MICACT – Microactuators" and by the Institutional Research Funding project IUT20-24 from the Estonian Research Council.

NOMENCLATURE

aC	Specific capacitance (F/m^3)
$c_{\pm}$	Concentration of cations and anions (mol/m^3)
C_i	Concentration (mol/m^3)
D_{eff}	Effective diffusion coefficient (m^2/s)
D_i	Diffusion coefficient (m^2/s)
e	Electron charge (C)
E	Young's modulus (Pa)
F	Faraday constant (C/mol)
i	Ionic species; either cations or anions (+ or −)
J_i	Ionic flux
L	Geometrical thickness of the electrode (m)
L'	Diffusion length of ions through the thickness direction (m)
r	Pore's characteristic dimension (m)
R	Gas constant [J/(K mol)]
T	Temperature (K)
u	Displacement vector (m)
u	Velocity of the flux flow (kg s^{-1} m^{-2})
V_{empty}	Volume of empty space (m^3)
V_T	Total volume of the electrode (m^3)
z_i	Charge of species i
β	Bruggeman exponent
δ	Active particle shape
ε	Permittivity of the medium (F/m)
ε	Strain
ε_{in}	Intercalation strain
ε_o	Permittivity of a vacuum (F/m)
η_e	Charge density (C/m^3)
μ	Dynamic viscosity (Pa s)
ρ	Active particle conductivity (S/m)
ρ_b	Effective ionic conductivity (S/m)
ρ_e	Effective active particle conductivity (S/m)
ρ_p	Density (kg/m^3)
σ	Stress (Pa)
σ_{in}	Intercalation stress (Pa)
σ_M	Mechanical stress (Pa)
σ_T	Total stress (Pa)
τ	Tortuosity
υ	Poisson's ratio
Φ_1, Φ_2	Potential at solid and solution phase, respectively (V)
$\in$	Porosity

[1]T. Wallmersperger, D. J. Leo, and C. S. Kothera, J. Appl. Phys. **101**, 024912 (2007).
[2]M. Shahinpoor and K. J. Ki, Smart Mater. Struct. **14**, 197–214 (2005).
[3]Z. Zhu, K. Asaka, L. Chang, K. Takagi, and H. Chen, J. Appl. Phys. **114**, 084902 (2013).
[4]V. Palmre, D. Brandell, U. Maeorg, J. Torop, O. Volobujeva, A. Punning, U. Johanson, M. Kruusmaa, and A. Aabloo, Smart Mater. Struct. **18**, 095028 (2009).
[5]W. Yang, H. Choi, S. Choi, M. Jeon, and S. Y. Lee, Smart Mater. Struct. **21**, 055012 (2012).
[6]B. J. Landi, R. P. Raffaelle, M. J. Heben, J. L. Alleman, W. VanDerveer, and T. Cennet, Nano Lett. **2**, 1329–1332 (2002).
[7]K. Mukai, K. Asaka, K. Kiyohara, T. Sugino, I. Takeuchi, T. Fukushima, and T. Aida, Electrochim. Acta **53**, 5555–5562 (2008).
[8]J. H. Jung, J. H. Jeon, V. Sridhar, and I.-K. Oh, Carbon **49**, 1279–1289 (2011).
[9]V. Palmre, E. Lust, A. Jänes, M. Koel, A. L. Peikolainen, J. Torop, U. Johanson, and A. Aabloo, J. Mater. Chem. **21**, 2577–2583 (2011).
[10]J. Torop, V. Palmre, M. Arulepp, T. Sugino, K. Asaka, and A. Aabloo, Carbon **49**, 3113–3119 (2011).
[11]J. Kim, S.-H. Bae, M. Kotal, T. Stalbaum, K. J. Kim, and I.-K. Oh, Small **13** (2017).
[12]M. Kotal, J. Kim, K. J. Kim, and I. K. Oh, Adv. Mater. **28**, 1610 (2016).
[13]B. J. Akle, M. D. Bennett, and D. J. Leo, Sens. Actuators, A **126**, 173–181 (2006).
[14]I. Must, V. Vunder, F. Kaasik, I. Põldsalu, U. Johanson, A. Punning, and A. Aabloo, Sens. Actuators, B **202**, 114–122 (2014).
[15]K. Kikuchi, T. Sakamoto, S. Tsuchitani, and K. Asaka, J. Appl. Phys. **109**, 073505 (2011).
[16]J. Kim, J. H. Jean, H. J. Kim, H. Lim, and I. K. Oh, ACS Nano **8**, 2986 (2014).
[17]J. Torop, Ph.D. thesis (University of Tartu, Estonia, 2012).
[18]K. M. Kim, N. G. Park, K. S. Ryu, and S. H. Chang, Electrochim. Acta **51**, 5636–5644 (2006).
[19]F. Kaasik, I. Must, I. Baranova, I. Poldsalu, E. Lust, U. Johanson, A. Punning, and A. Aabloo, Sens. Actuators, B **246**, 154–163 (2017).
[20]A. J. McDaid, *Ionic Polymer Metallic Composite Transducers for Biomedical Robotics Applications* (IFSA Publishing, Spain, 2014).
[21]T. Stalbaum, D. Pugal, S. E. Nelson, V. Palmre, and K. J. Kim, J. Appl. Phys. **117**, 114903 (2015).
[22]Z. Zhu, Y. Wang, Y. Liu, K. Asaka, X. Sun, L. Chang, and L. Pin, J. Appl. Phys. **120**, 034901 (2016).
[23]S. Nemat-Nasser and L. Jiang Yu, J. Appl. Phys. **87**(7), 3321–3331 (2000).
[24]M. Porfiri, Smart Mater. Struct. **18**(1), 015016 (2009).
[25]X. Wang and W. Hong, Appl. Phys. Lett. **98**, 081910 (2011).
[26]B. J. Akle, K. B. Wiles, D. J. Leo, and J. E. McGrath, Proc. SPIE **5385** (2004).
[27]L. Chang, K. Asaka, Z. Zhu, Y. Wang, H. Chen, and D. Li, J. Appl. Phys. **115**, 244901 (2014).
[28]V. Palmre, D. Pugal, K. K. Leang, and K. Kim, Proc. SPIE **8687** (2013).
[29]Q. Shen, V. Palmre, T. Stalbaum, and K. J. Kim, J. Appl. Phys. **118**, 124904 (2015).
[30]V. Vunder, M. Itik, I. Põldsalu, A. Punning, and A. Aabloo, Smart Mater. Struct. **23**, 025010 (2014).
[31]Y. Liu, R. Zhao, M. Ghaffari, J. Lin, S. Liu, H. Cebeci, R. Guzman de Villoria, R. Montazami, D. Wang, B. L. Wardle, J. R. Heflin, and Q. M. Zhang, Sens. Actuators, A **181**, 70–76 (2012).
[32]K. Kruusamäe, A. Punning, and A. Aabloo, Sensors **12**(2), 1950–1966 (2012).
[33]Z. Chen, D. Hedgepeth, and X. Tan, Smart Mater. Struct. **18**, 055008 (2009).
[34]A. A. Amiri Moghadam, T. Keivan, K. Akif, Z. Alam, M. N. Hisham, K. Abbas, and M. Bobak, Soft Rob. **3**(2), 82–97 (2016).
[35]A. Hunt, Z. Chen, X. Tan, and M. Kruusmaa, Smart Mater. Struct. **25**, 035016 (2016).
[36]J. W. Long, B. Dunn, D. R. Rolison, and H. S. White, Chem. Rev. **104**, 4463–4492 (2004).
[37]M. Ebner and V. Wood, J. Electrochem. Soc. **162**, A3064–A3070 (2015).
[38]J. Cannarella and C. Arnold, J. Power Sources **226**, 149–155 (2013).
[39]J. Ott, B. Völker, Y. Gan, R. M. McMeeking, and M. Kamlah, Acta Mech. Sin. **29**(5), 682–698 (2013).
[40]R. B. Smith, E. Khoo, and M. Z. Bazant, J. Electrochem. Soc. **164**, E3291 (2017).
[41]J. Newman and K. Thomas-Alyea, *Electrochemical Systems* (John Wiley and Sons, Inc., Hoboken, New Jersey, 2004).
[42]M. W. Verbrugge and P. Liu, J. Electrochem. Soc. **152**, D79 (2005).
[43]R. Drummond, D. A. Howey, and S. R. Duncan, J. Power Sources **277**, 317–328 (2015).
[44]H. Tavassol, E. M. Jones, N. R. Sottos, and A. A. Gewirth, Nat. Mater. **15**, 1182–1187 (2016).
[45]A. Punning, V. Vunder, I. Must, U. Johanson, G. Anbarjafari, and A. Aabloo, J. Intell. Mater. Syst. Struct. **27**, 1061–1074 (2016).
[46]C. Jenkins and S. Khanna, *Mechanics of Materials* (Elsevier Academic Press, 2005).
[47]C. L. Wong, A. N. Soriano, and M. H. Li, Fluid Phase Equilibr. **271**, 43–52 (2008).
[48]See http://www.sigmaaldrich.com/catalog/product/sial/04367?lang=en&region=EE for density and molar mass.
[49]M. G. Freire, A. R. R. Teles, M. A. A. Rocha, B. Schröder, C. M. S. S. Neves, P. J. Carvalho, D. V. Evtuguin, L. M. N. B. F. Santos, and J. A. P. Coutinho, J. Chem. Eng. Data **56**, 4813–4822 (2011).